Jue, T., Krishnamoorthi, R., & La Mar, G. N. (1983) *J. Am. Chem. Soc. 105*, 5701–5702.
Karplus, M., & McCammon, A. (1981) *CRC Crit. Rev. Biochem. 91*, 293–349.
La Mar, G. N., Smith, K. M., Gersonde, K., Sick, H., & Overkamp, M. (1980) *J. Biol. Chem. 255*, 66–70.
La Mar, G. N., Burns, P. D., Jackson, T. J., Smith, K. M., Langry, K. C., & Strittmatter, P. (1981) *J. Biol. Chem. 256*, 6075–6079.
La Mar, G. N., Davis, N. L., Parish, D. W., & Smith, K. M. (1983) *J. Mol. Biol. 168*, 887–896.
La Mar, G. N., Toi, H., & Krishnamoorthi, R. (1984) *J. Am. Chem. Soc. 106*, 6395–6401.
Lecomte, J. T. J., Johnson, R. D., & La Mar, G. N. (1985) *Biochim. Biophys. Acta* (in press).
Lindstrom, T. R., Noren, I. B. E., Charache, S., Lehmann, H., & Ho, C. (1972) *Biochemistry 11*, 1677–1681.
Livingston, D. J., Davis, N. L., La Mar, G. N., & Brown, W. D. (1984) *J. Am. Chem. Soc. 106*, 3025–3026.
Mayer, A., Ogawa, S., Shulman, R. G., Yamane, T., Cavaleiro, J. A. S., Rocha Gonsalves, A. M. d'A., Kenner, G. W., & Smith, K. M. (1974) *J. Mol. Biol. 86*, 749–756.
Nagai, K., Hori, H., Morimoto, H., Hayashi, A., & Taketa, F. (1979) *Biochemistry 18*, 1304–1308.
Neya, S., & Morishima, I. (1981) *J. Biol. Chem. 256*, 793–798.
Ondrias, M. R., Rousseau, D. L., Kitagawa, T., Ikeda-Saito, M., Inubushi, T., & Yonetani, T. (1982) *J. Biol. Chem. 257*, 8766–8770.
Perutz, M. F. (1970) *Nature (London) 228*, 726–739.
Perutz, M. F. (1976) *Br. Med. Bull. 32*, 195–208.
Potter, W. T., Hazzard, J. H., Kawanishi, S., & Caughey, W. S. (1983) *Biochem. Biophys. Res. Commun. 116*, 719–725.
Rose, M. Y., & Olson, J. S. (1983) *J. Biol. Chem. 258*, 4298–4303.
Smith, K. M., & Pandey, R. K. (1983) *J. Heterocycl. Chem. 20*, 1383–1388.
Smith, K. M., Fujinari, E. M., Langry, K. C., Parish, D. W., & Tabba, H. D. (1983) *J. Am. Chem. Soc. 105*, 6638–6646.
Teale, F. W. J. (1959) *Biochim. Biophys. Acta 35*, 543.

## *Articles*

# Vicinal Coupling Constants and Protein Dynamics†

Jeffrey C. Hoch‡
*The Rowland Institute for Science, Cambridge, Massachusetts 02142*
Christopher M. Dobson‡
*Inorganic Chemistry Laboratory, Oxford OX1 3QR, England*
Martin Karplus*
*Department of Chemistry, Harvard University, Cambridge, Massachusetts 02138*
*Received August 22, 1984; Revised Manuscript Received February 7, 1984*

ABSTRACT: The effects of motional averaging on the analysis of vicinal spin–spin coupling constants derived from proton NMR studies of proteins have been examined. Trajectories obtained from molecular dynamics simulations of bovine pancreatic trypsin inhibitor and of hen egg white lysozyme were used in conjunction with an expression for the dependence of the coupling constant on the intervening dihedral angle to calculate the time-dependent behavior of the coupling constants. Despite large fluctuations, the time-average values of the coupling constants are not far from those computed for the average structure in the cases where fluctuations occur about a single potential well. The calculated differences show a high correlation with the variation in the magnitude of the fluctuations of individual dihedral angles. For the cases where fluctuations involve multiple sites, large differences are found between the time-average values and the average structure values for the coupling constants. Comparison of the simulation results with the experimental trends suggests that side chains with more than one position are more common in proteins than is inferred from X-ray results. It is concluded that for the main chain, motional effects do not introduce significant errors where vicinal coupling constants are used in structure determinations; however, for side chains, the motional average can alter deductions about the structure. Accurately measured coupling constants are shown to provide information concerning the magnitude of dihedral angle fluctuations.

Scalar coupling constants between protons separated by three bonds have been widely used in the conformational analysis of amino acids and peptides by nuclear magnetic resonance (NMR) (Feeney, 1975; Bystrov, 1976). Both theoretical (Karplus, 1959, 1963) and experimental (Bystrov, 1976) investigations have demonstrated that the three-bond (vicinal) coupling constant between two protons can be described by an equation of the form

$$^3J_{H\text{-}H'} = A \cos^2 \theta + B \cos \theta + C \quad (1)$$

where $^3J_{H\text{-}H'}$ is the vicinal coupling constant, $\theta$ is the H–X–

† Supported in part by grants from the National Science Foundation and the National Institutes of Health and by the Rowland Institute for Science. C.M.D. is a member of the Oxford Enzyme Group.
‡ Work initiated while the author was at Harvard University.

0006-2960/85/0424-3831$01.50/0 

Y–H′ dihedral angle, and $A$, $B$, and $C$ are constants. The latter have been determined empirically for the various groups in polypeptides (Bystrov et al., 1973; Kopple et al., 1973) but can, in principle, be obtained from theoretical calculations (Barfield & Karplus, 1969).

Proton NMR spectra of proteins are considerably more complex than those of amino acids or peptides because of the large number of protons and the extensive overlap of many of the resonances. At present, extensive coupling constant data for proteins are limited to particularly well-studied molecules such as bovine pancreatic trypsin inhibitor (BPTI) (Dubs et al., 1979; Nagayama, 1981; Nagayama & Wüthrich, 1981) and hen egg white lysozyme (HEWL) (Delepierre et al., 1982; Delepierre, 1983). With the increasing use of methods for resolution and assignment including two-dimensional NMR spectroscopy (Campbell & Dobson, 1979; Nagayama, 1981; Wagner & Wüthrich, 1982), it is anticipated that more extensive sets of coupling constant data for a variety of proteins will become available.

With the assumption that a protein in solution is rigid and has the same structure as in the crystal, it is possible to calculate directly the vicinal couplings from crystallographically determined dihedral angles by using eq 1. There is, in general, reasonable correlation between coupling constants calculated in this way and the limited experimental data which are available (Nagayama & Wüthrich, 1981; Delepierre et al., 1982). Although a considerable body of data suggests that average solution structures are similar to crystal structures (Dobson, 1977, 1982; Wüthrich et al., 1978; Poulsen et al., 1980; Nagayama & Wüthrich, 1981), it is well established that proteins are not rigid and undergo a variety of significant structural fluctuations about the average structure (Karplus & McCammon, 1981, 1983). Of particular interest in this regard is the fact that protein simulations (van Gunsteren & Karplus, 1982; Northrup et al., 1981), as well as temperature factor data (Artymiuk et al., 1979; Frauenfelder et al., 1979), show clearly that the magnitudes of positional fluctuations increase as one moves out along a side chain. Dihedral angle fluctuations, which depend on the correlations of atomic motions that are not directly accessible to X-ray determination, are also shown by simulations to increase outward along side chains. Since vicinal coupling constants depend on the dihedral angles according to eq 1, it is of interest to investigate the effect of dihedral angle fluctuations on vicinal coupling constant values. For this purpose, we use molecular dynamic simulations for BPTI (van Gunsteren & Karplus, 1982) and HEWL (T. Ichiye, B. Olafson, and M. Karplus, unpublished results). We examine to what extent the level of agreement between observed coupling constants and the values calculated from a rigid crystal structure allows limits to be placed on the possible magnitudes of dihedral angle fluctuations in a protein. In addition, we examine whether the level of agreement can be improved by consideration of specific protein motions, and hence whether coupling constant data can be used to provide information on the magnitude of dihedral angle fluctuations.

The general procedure employed is that used in a previous investigation of motional averaging effects on ring current chemical shifts in BPTI (Hoch et al., 1982). Vicinal coupling constants were computed for each coordinate set comprising the molecular dynamics trajectory. From these, the fluctuations, distributions, and average values of the coupling constants were obtained. Although the subpicosecond fluctuations in the coupling constants computed from the simulations are not experimentally accessible, the calculated fluctuations provide insight into the process of motional averaging. A comparison of time-average values with the coupling constants computed from the average structure serves to illustrate the influence of dynamics.

The analysis of the nature of motional averaging of coupling constants is more straightforward than that for chemical shifts. The coupling constants depend primarily on a single variable, the dihedral angle between protons. The chemical shifts, even when only the ring current contribution is considered, depend on two parameters, the distance of a proton from an aromatic ring and the angle formed by a vector normal to the ring plane and a vector connecting the ring center and the proton. The dihedral angle gives a simpler characterization of local structure and motion than do proton–ring distances and angles. Another factor is that the theory of vicinal coupling constants is considerably more complete than is that of chemical shifts in proteins.

## Materials and Methods

Provided the time scale of the dihedral angle fluctuations is fast compared to the NMR time scale, the measured value of the vicinal proton coupling constants, $^3J_{H-H}$, is a Boltzmann average over the coupling constant values, $J(\theta)$, as a function of the dihedral angle, $\theta$

$$^3J_{H-H'} = \int_0^{2\pi} J(\theta)P(\theta)\, d\theta \qquad (2)$$

where $P(\theta)$ is the equilibrium probability of obtaining the angle $\theta$ at a temperature $T$. Since in solution, or in the interior of a protein, the surrounding medium affects the form of $P(\theta)$, we have

$$P(\theta) = e^{-W(\theta)/kT} \qquad (3)$$

where $W(\theta)$ is the potential of mean force, which includes the effect of the dihedral angle potential of the isolated system and the average effect of the surroundings (McQuarry, 1976). The molecular dynamics simulation, in principle, determines $W(\theta)$ and, therefore, the correct form of $P(\theta)$, in contrast to the isolated molecule potentials that are normally used for obtaining average values of coupling constants (Tonelli et al., 1970; Gibbons et al., 1970).

In the present study, we make use of the results of molecular dynamics simulations of BPTI and HEWL to investigate the nature and extent of the motional averaging of vicinal coupling constants. Thus, the phase space average in eq 2 is replaced by a time average over the trajectory. Values for vicinal coupling constants are computed for each coordinate set comprising the molecular dynamics trajectory, and the average of these values is then obtained. These are compared with the coupling constants computed directly from the average coordinates obtained in the simulation. The difference between the two gives a direct measure of the dynamical effects on the coupling constants and circumvents any complications due to differences between the dynamic average structure and the X-ray or solution structure. In addition to the average values of the coupling constant and the distributions on which they are based, the coupling constant fluctuations are obtained from the trajectory.

Three different molecular dynamics trajectories were used in this investigation. Two of the trajectories, denoted VAC and SOLV, are from simulations of BPTI (van Gunsteren & Karplus, 1982). The third is from a simulation of lysozyme and is denoted HEWL (T. Ichiye et al., unpublished results). All three of the simulations were carried out in the extended atom approximation in which hydrogen atoms are not considered explicitly, but their presence is accounted for by adjusting the mass and van der Waals radius of the directly

Table I: Coupling Constant Fluctuations[a]

| | trajectory | | | | | |
|---|---|---|---|---|---|---|
| | SOLV | | VAC | | HEWL | |
| torsion angle | no.[b] | rms fluctuation | no. | rms fluctuation | no. | rms fluctuation |
| $\phi$ | 59 (59) | 1.57 (1.57) | 59 (57) | 1.49 (1.46) | 138 (127) | 1.66 (1.57) |
| $\chi_1$ | 78 (65) | 1.61 (1.33) | 78 (58) | 1.90 (1.36) | 187 (140) | 1.89 (1.51) |
| $\chi_2$ | 64 (30) | 2.74 (2.22) | 64 (40) | 2.32 (1.82) | 124 (80) | 2.19 (1.84) |
| $\chi_3$ | 40 (32) | 2.61 (2.53) | 40 (20) | 2.47 (1.74) | 68 (40) | 2.67 (2.32) |
| $\chi_4$ | 16 (8) | 3.27 (3.16) | 16 (4) | 3.11 (2.00) | 24 (16) | 2.85 (2.46) |
| overall | 257 (194) | 2.14 (1.82) | 257 (179) | 2.07 (1.55) | 541 (403) | 2.04 (1.71) |

[a] Proline is excluded. The units of the fluctuations are hertz. [b] Number refers to the number of coupling constant values considered for each dihedral angle; numbers in parentheses are for unimodal torsion angle distributions (see text).

bonded atoms. Both of the BPTI simulations were carried out for 25 ps, with an average temperature of 301 K. The SOLV simulation differs from the VAC run in that BPTI was surrounded by a box of Lennard–Jones solvent "molecules", and the equations were solved for the entire system (protein plus solvent with periodic boundary conditions) to simulate the influence of solvent on the motion. The HEWL simulation was carried out for 33 ps, with an average temperature of 300 K. Detailed descriptions of the simulations are given elsewhere [van Gunsteren & Karplus, 1982; T. Ichiye et al., unpublished results; for a general description of the methodology, see Brooks et al. (1983)].

For each calculation, a subset of the complete trajectory was used in the coupling constant analysis. From the two BPTI trajectories, configurations of the protein at 0.08-ps intervals were used, for a total of 312 configurations. From the lysozyme trajectory, 330 configurations, spaced at 0.1-ps intervals, were used. Proton coordinates for each configuration of the protein were generated as described previously (Hoch et al., 1982). Comparisons between calculations using the extended atom model and calculations in which all atoms are explicitly treated have shown that the computed constants are not significantly affected by the extended atom approximation (Hoch, 1983). In the extended atom approximation, the configuration of the non-hydrogen atoms uniquely determines the interproton torsion angles in most cases; exceptions are those involving methyl groups. The internal dynamics of methyl groups are not available from simulations involving extended atoms, so the molecular dynamics trajectories could not be used to study coupling constants involving methyl groups. Methyl coupling constants are, in any case, relatively insensitive to dynamics.[1] Including all other main-chain and side-chain protons, there are a total of 297 vicinal coupling constants for BPTI and 561 for HEWL, all of which were calculated from the molecular dynamics trajectories. The specific examples of dynamic coupling constant behavior are taken from the SOLV trajectory, though corresponding results are found in all three trajectories.

Two sets of parameters $A$, $B$, and $C$ were used in conjunction with eq 1 to compute the coupling constants. The values 9.4, −1.1, and 0.4 Hz, respectively (Bystrov et al., 1973), were used for $H^N$–$H^\alpha$ couplings (which depend on the torsion angle $\phi$). A correction for electronegativity effects was applied by dividing the values obtained from eq 1 by 1.09 (Bystrov et al., 1973). The values 9.4, −1.4, and 1.6 Hz (Kopple et al., 1973) were used for the side-chain coupling constants. Electronegativity corrections for side-chain couplings are smaller than the $H^N$–$H^\alpha$ corrections and were not applied (Kopple et al., 1973; Bystrov, 1976). Similar values of the parameters $A$, $B$, and $C$ have been suggested by De Marco et al. (1978) and Cung & Marraud (1982). Equation 1 is plotted in Figure 1 for both sets of parameters.

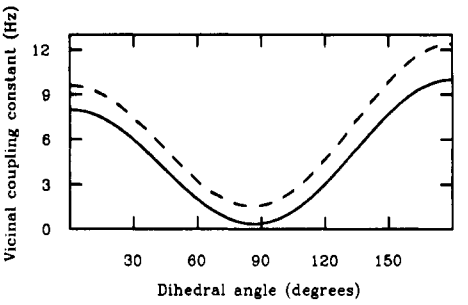


FIGURE 1: Equation 1 with $A$, $B$, and $C$ equal to 9.4, −1.4, and 1.6 (solid line) for side chains and 9.4, −1.1, and 0.4 for the main chain, respectively, corrected for electronegativity effects (dashed line).

In addition to torsion angles and substituent electronegativity, there are other factors which are known to influence vicinal coupling constants. Among these are bond angle and bond length variations (Karplus, 1963). Their effect on motional averaging of coupling constants cannot be assessed in the present study because of the use of the extended atom approximation. In any case, the main results of the present investigation are not dependent on the exact values used for the parameters.

Atoms are named according to IUPAC–IUB convention (IUPAC–IUB, 1970). Torsion angles defined by the non-hydrogen atoms are referred to by their normal designations ($\phi$, $\chi_1$, $\chi_2$, etc.). Dihedral angles between hydrogen atoms are referred to by designating the two hydrogen atoms involved. No ambiguity arises because hydrogen atom names are derived from the directly bonded non-hydrogen atom (e.g., $H^\alpha$ is bonded to $C^\alpha$). Vicinal coupling constants are designed by the hydrogen atoms which are coupled (e.g., $J_{\alpha\beta}$ for the $H^\alpha$–$H^\beta$ coupling).

## RESULTS

Two aspects of the coupling constants computed from the simulations are considered here. The first involves examination of the nature of the fluctuations and their average values. The second concerns the implication of the results for experimental studies of proteins. Available experimental data are examined in light of this analysis.

*Analysis of Coupling Constants Derived from Simulations. (a) Nature of Coupling Constant Fluctuations.* The root mean square (rms) fluctuations in the coupling constants derived from the SOLV trajectory range in magnitude from 0.3 to 4.7 Hz. Results for the three trajectories are summarized in Table I. The average coupling constant fluctuation for all three trajectories is approximately 2 Hz. The largest rms fluctuation computed from the SOLV trajectory for the coupling constant

[1] Assuming only that the three protons of a methyl group are separated by an angle of 120° and that they undergo rapid exchange, the average $J$ value is independent of the dihedral angle distribution for the methyl group; it is equal to $A/2 + C$.

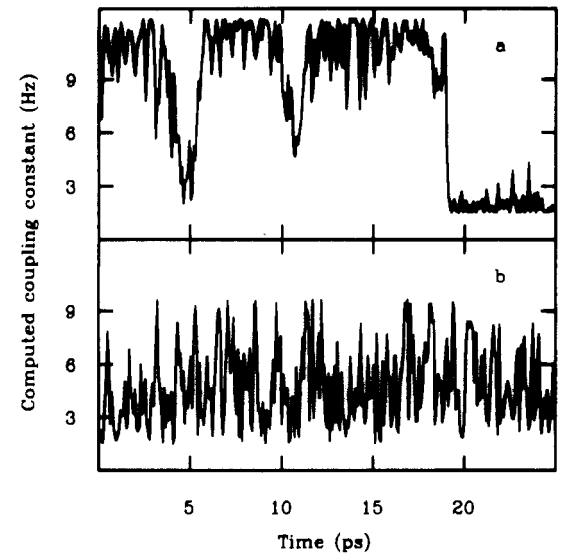


FIGURE 2: Time evolution of coupling constants computed from the simulation: (a) Glu-7 $J_{\beta_1\gamma_1}$; (b) Arg-42 $J_{\beta_1\gamma_1}$.

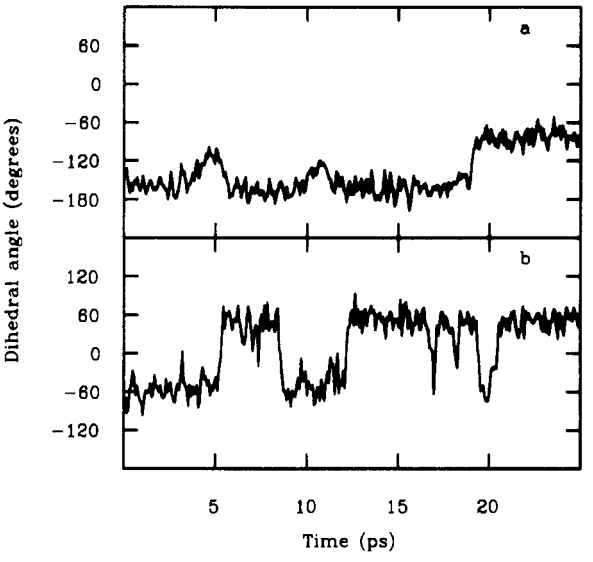


FIGURE 3: Time evolution of interproton dihedral angles computed from the simulation: (a) Glu-7 $\theta_{\beta_1\gamma_1}$; (b) Arg-42 $\theta_{\beta_1\gamma_1}$.

$J_{N\alpha}$, corresponding to the main-chain torsion angle $\phi$, is 2.7 Hz. For the side-chain torsion angles ($\chi_1 \rightarrow \chi_4$), there are 91 coupling constants with rms fluctuations larger than 2.7 Hz. It is apparent that the coupling constant fluctuations generally increase outward along the side chain.

Examination of the explicit time course of some of the computed coupling constants and of the corresponding torsion angles reveals that fluctuations in the coupling constants arise from two types of behavior. High-frequency fluctuations ($\sim 10^{12}$ s$^{-1}$) result from torsional oscillations within a particular potential well, or rotamer. Lower frequency fluctuations ($\sim 10^{11}$ s$^{-1}$ or slower) arise from transitions between rotamers. Both types of fluctuations are evident in the time course of $J_{\beta_1\gamma_1}$ of Glu-7 (Figures 2a and 3a) and Arg-42 (Figures 2b and 3b). Transitions between rotamers are relatively rare events on the time scale of the simulations (Campbell et al., 1976; van Gunsteren & Karplus, 1982). Consequently, the relative populations of the rotamers may not be statistically significant, and coupling constants which depend on torsion angles undergoing such relatively rare events are likely to be incompletely averaged. Since for $\chi_2$ through $\chi_4$ 50 out of the 120 dihedral angles underwent at least one rotational transition, it is evident that this type of motion is significant for averaging coupling constants. In all 15 cases where the rms fluctuation exceeds 4 Hz, the corresponding torsion angle is distributed about more than one rotamer.

Table II: Illustrative Coupling Constant Statistics[a]

| residue | coupling constant | time average | average structure | difference | rms fluctuation |
|---|---|---|---|---|---|
| Glu-7 | $\beta_1\gamma_1$ | 8.23 | 7.95 | 0.28 | 4.08 |
| Pro-9 | $\beta_1\gamma_1$ | 7.66 | 9.49 | 1.83 | 1.27 |
| Ile-19 | $N\alpha$ | 5.28 | 5.33 | 0.05 | 2.07 |
| Cys-30 | $\alpha\beta_1$ | 10.69 | 11.01 | 0.32 | 1.42 |
| | $\alpha\beta_2$ | 1.93 | 1.55 | 0.38 | 0.48 |
| Arg-42 | $\beta_1\gamma_1$ | 7.88 | 5.71 | 2.17 | 4.23 |

[a] Computed from the molecular dynamics simulation and eq 1 with parameters given in the text. All units are hertz.

To distinguish the effects of such transitions from the effects of rapid motional averaging within a rotamer, statistics were computed excluding all coupling constants for which the corresponding torsion angle distribution is not unimodal. These statistics appear in parentheses in Table I. While the magnitudes of the computed fluctuations are smaller than the magnitudes computed by using all coupling constants, the overall trends are the same.

The coupling constant fluctuations depend on the corresponding torsion angle fluctuations, but there is an additional structural factor since the magnitude of the coupling constant fluctuations depends also on the mean value, $\bar{\theta}$, of the corresponding torsion angle about which the fluctuations occur. For small changes in the dihedral angle from the mean, $\Delta\theta$, the corresponding change in the coupling constant, $\Delta J$, is

$$\Delta J = \left[\frac{\partial J(\theta)}{\partial \theta}\right]_{\bar{\theta}} \Delta\theta \qquad (4)$$

The influence of the factor $[\partial J(\theta)/\partial\theta]_{\bar{\theta}}$ manifests itself as a difference in the magnitude of coupling constant fluctuations for coupling constants with similar dihedral angle fluctuations but different values of $\bar{\theta}$. For example, the $J_{\alpha\beta_1}$ and $J_{\alpha\beta_2}$ coupling constants which correspond to dihedral angles that undergo the same fluctuations in the present model result in different coupling constant fluctuations because $\bar{\theta}$ differs by 120°. The difference in behavior is illustrated by the result for Cys-30 given in Table II. The effect is also evident in the time course of the Glu-7 $\chi_2$ fluctuation. The dihedral angle fluctuations in the time intervals 12–17 and 20–25 ps are of similar magnitudes (Figure 3a), but the coupling constant fluctuations during the former interval are considerably larger (Figure 2a); this is in accord with the approximate values of $[\partial J/\partial\theta]_{\bar{\theta}}$ for the two intervals (5.1 and 3.3, respectively). The influence of the term $[\partial J/\partial\theta]_{\bar{\theta}}$ on the magnitude of coupling constant fluctuations for cases with unimodal dihedral angle distributions is evident as a general trend when the fluctuations are correlated with the value of the mean dihedral angle (Figure 4a). The trend mirrors closely the dependence of $[\partial J/\partial\theta]_{\bar{\theta}}$ on the value of the dihedral angle (Figure 4b).

Fluctuations for coupling constants with bi- or multimodal dihedral angle distributions are generally larger, on average, and reflect the variation of $[\partial J/\partial\theta]_{\bar{\theta}}$ with $\bar{\theta}$ to a lesser extent. However, there are circumstances under which transitions between rotamers do not produce large coupling constant fluctuations. This arises primarily from the fact that a coupling constant is independent of the sign of the corresponding dihedral angle. For example, transitions of the type $\theta = -60°$ to $\theta = +60°$ have no effect on the coupling constant. This is illustrated by the time course of $J_{\beta_1\gamma_1}$ and the corresponding

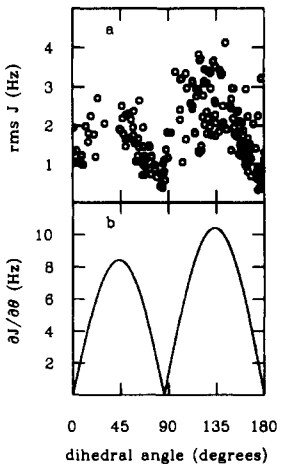


FIGURE 4: Angular dependence of coupling constant fluctuations: (a) root mean square fluctuations of $J$ as a function of $\bar{\theta}$ for residues with unimodal $\theta$ distributions; (b) $\partial J/\partial\theta$ vs. $\theta$, obtained by differentiating eq 1 with $A$, $B$, and $C$ equal to 9.4, −1.4, and 1.6, respectively.

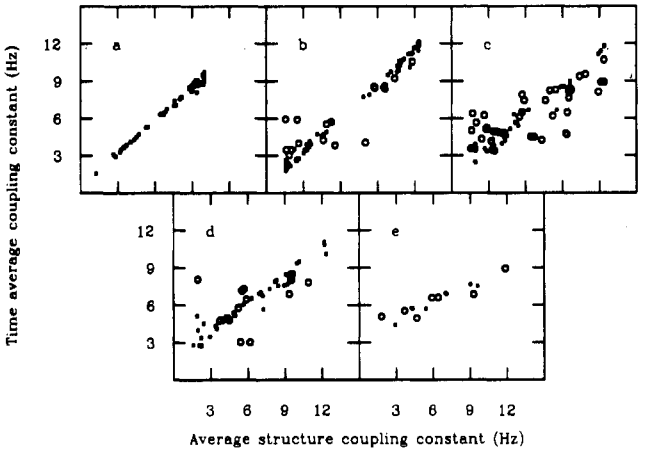


FIGURE 5: Comparison of time-average and average structure coupling constants computed from the SOLV simulation for coupling constants associated with (a) $\phi$, (b) $\chi_1$, (c) $\chi_2$, (d) $\chi_3$, and (e) $\chi_4$. Small filled circles indicate the corresponding dihedral angle distribution is unimodal; open circles indicate multimodal distributions.

dihedral angle of Arg-42 (Figures 2b and 3b).

(*b*) *Average Values.* The influence of dynamics on the average values of the coupling constants can be examined by comparing the time-average results with those computed from the average structure of the protein obtained from the simulation. Experimental coupling constants are time averages, while an X-ray crystal structure corresponds to an average structure. Consequently, the comparison of time-average and average structure coupling constants from the simulations probes the expected relationship between experimental coupling constants and coupling constants computed from crystal structure data.

Differences in the coupling constants from the two types of averages range in magnitude from 0 to 6 Hz for the SOLV trajectory. As was observed for the fluctuations, the largest differences arise from bi- or multimodal dihedral angle distributions. For unimodal angular distributions, the largest coupling constant difference is 2 Hz. The results are shown in Figure 5; unimodal distributions are indicated by small circles and multimodal distributions by large circles. Two trends emerge from the comparison of time-average and average structure coupling constants. The first trend is that for large coupling constants (>8 Hz), the average structure value tends to exceed the time-average value, while for small coupling constants (<6 Hz) the reverse is true. The second trend

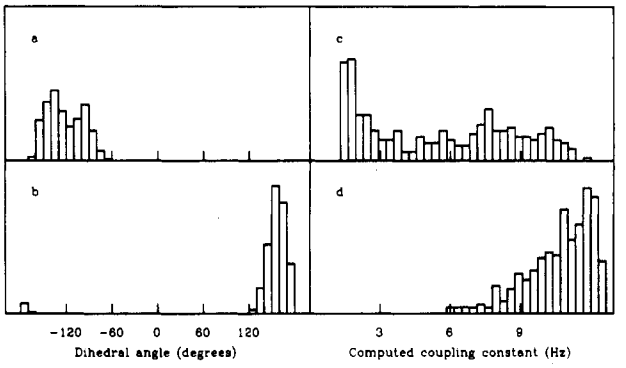


FIGURE 6: Dihedral angle and coupling constant distributions computed from the simulation: (a) Pro-9 $\theta_{\beta_1\gamma_1}$; (b) Cys-30 $\theta_{\alpha\beta_1}$; (c) Pro-9 $J_{\beta_1\gamma_1}$; (d) Cys-30 $J_{\alpha\beta_1}$.

is that the effect is larger for side-chain than for main-chain couplings and increases as one progresses out along the side chain. A measure of both of these trends is the slope of a least-squares line fitted to the data of Figure 5. Excluding coupling constants with bi- or multimodal torsion angle distributions, the slopes are 0.89, 0.88, 0.78, 0.78, and 0.71 for coupling constants corresponding to $\phi$, $\chi_1$, $\chi_2$, $\chi_3$, and $\chi_4$, respectively.

The first trend is explicable in terms of the angular dependence of the coupling constant (Figure 1). The form of the coupling constant distribution is determined by the corresponding dihedral angle distribution, $P(\theta)$, and eq 1. When a local extremum of eq 1 is within the range spanned by the dihedral angle distribution, a coupling constant distribution results which differs significantly from the dihedral angle distribution, since different portions of the dihedral angle distribution map to the same values of the coupling constant. The result is a coupling constant distribution which resembles the dihedral angle distribution folded about the value corresponding to the local extremum in eq 1. Examples of the resulting asymmetric distributions are shown for $J_{\alpha\beta_1}$ of Pro-9 (Figure 6a,c) and $J_{\alpha\beta_1}$ of Cys-30 (Figure 6b,d). The time-average coupling constant will be weighted toward small values when the dihedral angle distribution spans a local maximum, and toward large values for a local minimum, relative to the average structure value of the coupling constant (which is close to the value computed from the average torsion angle when the dihedral angle distribution is unimodal). The second trend reflects the magnitude of the corresponding dihedral angle fluctuations. Broader dihedral angle distributions result in larger differences between the time-average and average structure coupling constants. For example, in the limiting case of complete averaging, corresponding to a uniform torsion angle distribution, the two $\alpha\beta$ coupling constants average to the same value of 6.3 Hz.

When the dihedral angle distributions are not unimodal, much larger differences between the two methods of computing average coupling constants are obtained, in general (Figure 5). The differences reflect mainly the positions and relative populations of the rotamers. Multimodal dihedral angle distributions obtained in the simulations, while not necessarily correct because of the limited number of transitions, are illustrative of the large influence that multiple sites may have on the average values of coupling constants.

Differences between time-average torsion angles and torsion angles computed from the average structure behave similarly; that is, unimodal torsion angle distributions give rise to small differences, while multimodal distributions can produce large differences. For unimodal torsion angle distributions, the differences between the average structure and the time-average

Table III: Analysis of $\alpha\beta_1$ and $\alpha\beta_2$ Coupling Constant Pairs in Terms of Single-Site and Gaussian Model Distributions[a]

| | | | | | single site | | Gaussian | | |
|---|---|---|---|---|---|---|---|---|---|
| residue | $J_{\alpha\beta_1}$ | $J_{\alpha\beta_2}$ | $\langle\chi_1\rangle$ | $\langle\Delta\chi_1^2\rangle^{1/2}$ | $\chi_1^{fit}$ | $F(\chi_1^{fit})$ | $\chi_1^{fit}$ | $\sigma$ | $F(\chi_1^{fit}, \sigma)$ |
| Arg-1 | 5.9 | 3.8 | 5[b] | 68 | −113 | 0.05 | 81 | 33 | 0.00 |
| | | | | | | | −113 | 11 | 0.00 |
| Pro-2 | 4.1 | 8.6 | 4 | 18 | 4 | 0.92 | 8 | 19 | 0.00 |
| | | | | | | | −153 | 36 | 0.00 |
| Asp-3 | 10.8 | 1.9 | −80 | 11 | −83 | 0.11 | −81 | 11 | 0.00 |
| Phe-4 | 4.7 | 2.7 | 71 | 11 | 69 | 0.22 | 70 | 15 | 0.00 |
| Cys-5 | 12.1 | 3.2 | −61 | 11 | −60 | 0.09 | −62 | 10 | 0.00 |
| Leu-6 | 9.7 | 2.6 | −87 | 21 | 108 | 0.33 | −86 | 21 | 0.00 |
| | | | | | −92 | 0.90 | 108 | 0 | 0.33 |
| Glu-7 | 2.6 | 9.8 | −155 | 20 | 12 | 0.44 | −155 | 21 | 0.00 |
| | | | | | −148 | 0.94 | 12 | 0 | 0.44 |
| Pro-8 | 5.7 | 8.6 | −5[b] | 20 | −7 | 0.78 | 161 | 42 | 0.00 |
| | | | | | | | −4 | 21 | 0.00 |
| Pro-9 | 5.5 | 8.4 | −3[b] | 22 | −6 | 1.25 | −2 | 23 | 0.00 |
| | | | | | | | 168 | 47 | 0.00 |
| Tyr-10 | 2.2 | 10.1 | −156 | 17 | −151 | 0.39 | −155 | 16 | 0.00 |
| | | | | | 13 | 1.25 | | | |
| Pro-13 | 3.9 | 8.5 | -9 | 19 | 6 | 1.04 | 10 | 20 | 0.00 |
| | | | | | | | −150 | 33 | 0.00 |
| Cys-14 | 12.0 | 2.8 | −65 | 10 | −65 | 0.11 | −66 | 10 | 0.00 |
| Lys-15 | 7.7 | 2.7 | −101 | 11 | −104 | 0.09 | 96 | 18 | 0.00 |
| | | | | | 96 | 0.94 | −102 | 13 | 0.00 |
| Arg-17 | 11.2 | 2.3 | −73 | 16 | −78 | 0.39 | −75 | 14 | 0.00 |
| Arg-20 | 11.9 | 3.5 | −60 | 15 | −58 | 0.23 | −60 | 13 | 0.00 |
| Tyr-21 | 4.6 | 4.9 | −118 | 9 | −121 | 0.02 | −121 | 8 | 0.00 |
| | | | | | | | 56 | 38 | 0.00 |
| Phe-22 | 4.7 | 2.6 | 70 | 9 | 69 | 0.15 | 70 | 13 | 0.00 |
| Tyr-23 | 3.4 | 12.1 | 178 | 8 | 179 | 0.08 | 180 | 10 | 0.00 |
| Asn-24 | 2.1 | 9.7 | −151 | 14 | −148 | 0.21 | −151 | 14 | 0.00 |
| | | | | | 15 | 0.70 | 15 | 0 | 0.70 |
| Lys-26 | 10.6 | 3.0 | −77[b] | 25 | 112 | 1.56 | −74 | 22 | 0.00 |
| | | | | | −84 | 2.09 | | | |
| Leu-29 | 5.9 | 4.0 | 19[b] | 59 | −114 | 0.12 | 82 | 35 | 0.00 |
| | | | | | | | −113 | 15 | 0.00 |
| Cys-30 | 10.7 | 1.9 | −83 | 12 | −84 | 0.11 | −82 | 11 | 0.00 |
| Gln-31 | 11.2 | 2.0 | −77 | 12 | −79 | 0.12 | −78 | 10 | 0.00 |
| Phe-33 | 2.6 | 12.1 | −175 | 7 | −173 | 0.03 | −173 | 7 | 0.00 |
| Tyr-35 | 2.2 | 11.7 | −167 | 10 | −167 | 0.07 | −169 | 9 | 0.00 |
| Cys-38 | 3.7 | 3.6 | 62 | 12 | 60 | 0.32 | 61 | 17 | 0.00 |
| Arg-39 | 9.5 | 2.4 | −84 | 19 | 106 | 0.25 | −89 | 18 | 0.00 |
| | | | | | −93 | 0.50 | 106 | 0 | 0.25 |
| Lys-41 | 10.2 | 2.3 | −83 | 18 | −88 | 0.54 | −84 | 17 | 0.00 |
| | | | | | 107 | 1.34 | | | |
| Arg-42 | 3.5 | 9.2 | −147[b] | 29 | 8 | 0.05 | −156 | 30 | 0.00 |
| | | | | | | | 9 | 9 | 0.00 |
| Asn-43 | 2.7 | 12.2 | −177 | 8 | −175 | 0.01 | −174 | 6 | 0.00 |
| Asn-44 | 1.8 | 10.6 | −156 | 9 | −155 | 0.06 | −156 | 9 | 0.00 |
| Phe-45 | 11.4 | 3.9 | −53 | 19 | −53 | 0.79 | −58 | 19 | 0.00 |
| Lys-46 | 4.2 | 4.0 | 72[b] | 28 | −119 | 0.61 | 61 | 26 | 0.00 |
| | | | | | 61 | 1.44 | −119 | 0 | 0.61 |
| Ser-47 | 3.4 | 3.9 | 59 | 15 | 58 | 0.31 | 57 | 17 | 0.00 |
| Glu-49 | 3.5 | 7.9 | −141 | 26 | −135 | 1.19 | 17 | 23 | 0.00 |
| | | | | | 14 | 2.05 | −141 | 26 | 0.00 |
| Asp-50 | 4.7 | 5.7 | −122 | 22 | −123 | 0.57 | 41 | 43 | 0.00 |
| | | | | | | | −124 | 22 | 0.00 |
| Cys-51 | 2.1 | 10.4 | −155 | 14 | −154 | 0.30 | −157 | 14 | 0.00 |
| Met-52 | 3.5 | 8.4 | −140[b] | 28 | 11 | 0.98 | −146 | 28 | 0.00 |
| | | | | | −138 | 1.76 | 13 | 19 | 0.00 |
| Arg-53 | 11.3 | 2.2 | −74 | 14 | −77 | 0.24 | −76 | 12 | 0.00 |
| Cys-55 | 10.2 | 2.1 | −81 | 14 | −88 | 0.29 | −85 | 14 | 0.00 |

[a] Units are hertz for $J_{\alpha\beta_1}$ and $J_{\alpha\beta_2}$, degrees for $\langle\chi_1\rangle$, $\langle\Delta\chi_1^2\rangle^{1/2}$, $\chi_1^{fit}$, and $\sigma$, and hertz squared for $F(\chi_1^{fit})$ and $F(\chi_1^{fit}, \sigma)$. [b] The $\chi_1$ distribution is multimodal.

torsion angle were all less than 3° for the two BPTI simulations. For multimodal distributions, differences up to 48° were obtained, although most were less than 10°.

*Implications for Experimental Studies. (a) Analysis of Coupling Constant Values.* The calculation of dihedral angles directly from experimental coupling constants is hampered by two ambiguities: one arises because eq 1 is not single-valued on the interval 0–180° and the other because the coupling constant is independent of the sign of the corresponding dihedral angle. When two coupling constants are known whose dihedral angles are fixed relative to one another by geometry, these ambiguities are removed. This is the situation for $\alpha\beta_1$ and $\alpha\beta_2$ coupling constants, for example, when stereochemical assignments of the $\beta$-protons are known. Although stereochemical assignments are not easily made, the influence of protein dynamics can best be illustrated by focusing on a case where maximum information is available. In what follows, we therefore focus on $\alpha\beta_1$ and $\alpha\beta_2$ coupling constants. A complementary discussion which treats the experimental data for BPTI has been given by Nagayama & Wüthrich (1981).

Table III presents the results for the $J_{\alpha\beta_1}$ and $J_{\alpha\beta_2}$ values and dihedral angles obtained from the SOLV simulation and its analysis. Columns 2–5 give the calculated average values of $J_{\alpha\beta_1}$ and $J_{\alpha\beta_2}$ and the average dihedral angle values as well as their rms fluctuations. The remaining columns correspond to results obtained by using $J_{\alpha\beta_1}$ and $J_{\alpha\beta_2}$ as the "experimental" coupling constants and fitting them by procedures described below. An essential difference between the present analysis and that of experimental data is that the actual average values and the distributions are known for the angles from the simulation, while from experiment one has at best an estimate of the average angle from the crystal structure.

It is often the case in the simulations that the dihedral angles of side chains, particularly those in the protein interior, are symmetrically distributed about a single value of the dihedral angle (which does not necessarily correspond to one of the staggered configurations). For the SOLV trajectory, 32 of 40 $\chi_1$ torsion angles for residues with a $\beta$-methylene group exhibit such clearly unimodal distributions. The remainder exhibit asymmetric or multimodal distributions. Consequently, a single-site model is the simplest first approximation to the actual dihedral angle distributions in proteins. The appropriateness of a single-site model can be tested by analyzing the time-average coupling constants from the simulation in terms of a single dihedral angle and comparing the results with the actual dihedral angle distributions. In practice, experimental uncertainty (both in the measured $J$ values and in the empirical parameters in eq 1) means that a range of dihedral angles fits the coupling constants to within experimental error, rather than a single value. For $\alpha$-protons coupled to $\beta$-methylene groups, the range of dihedral angles is determined by finding the values of $\chi_1$ for which the trial function, or goodness of fit

$$F(\chi_1) = [J_{\alpha\beta_1} - J(\chi_1 - 120°)]^2 + [J_{\alpha\beta_2} - J(\chi_1)]^2 \quad (5)$$

has a value below a threshold corresponding to the experimental error. Here, $J_{\alpha\beta_1}$ and $J_{\alpha\beta_2}$ are the time-average coupling constants from the simulation, and $J(\chi_1 - 120°)$ and $J(\chi_1)$ are computed by using eq 1. If the experimental uncertainty in a single coupling constant measurement is ±0.5 Hz, the appropriate threshold value is 1 $Hz^2$.

Assuming a single site distribution, the results can be analyzed most simply by using eq 5 to find the best fit to the time-average coupling constants $J_{\alpha\beta_1}$ and $J_{\alpha\beta_2}$ with a single fixed value of $\chi_1$. Table III lists for each residue with an $\alpha$-proton coupled to a $\beta$-$CH_2$ group the resulting value of $\chi_1$, called $\chi_1^{fit}$, and the minimum values of the trial function, $F(\chi_1^{fit})$, in columns 6 and 7, respectively. In only four cases does the minimum value of eq 5 exceed 1.0 $Hz^2$, indicating that there is no single value of $\chi_1$ which yields $\alpha\beta_1$ and $\alpha\beta_2$ coupling constants within experimental error limits of the time-average coupling constants. For two of these cases, the corresponding $\chi_1$ distribution in the simulation is multimodal (Pro-9, Lys-26). In the other two cases, the $\chi_1$ distributions are very broad (Glu-49) or very asymmetric (Pro-13).

There are some cases in which eq 5 exhibits local minima which are indistinguishable, to within experimental uncertainty, from the global minimum on the basis of goodness of fit. The goodness of fit and the corresponding $\chi_1$ values for these local minima are listed as additional entries in columns 6 and 7 of Table III.

Unlike actual experiments, the simulation results permit a direct comparison between the value of $\langle\chi_1\rangle$ and that obtained from fitting the coupling constants. It is clear from Table III that in most cases the correspondence is quite good, particularly for cases where no ambiguity arises. In the left panel

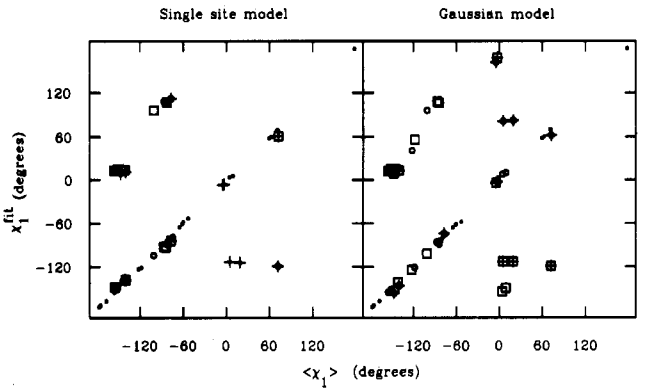


FIGURE 7: Values of $\chi_1$ which give the best fit of eq 1 to the time-average coupling constant computed from the simulation vs. $\langle\bar{\chi}_1\rangle$ from the simulation: (left panel) single-site model; (right panel) Gaussian model. Small filled circles indicate that a single fit was obtained; large circles and squares indicate global and local minima, respectively, when more than one close fit was obtained; an inscribed + indicates that the corresponding $\chi_1$ distribution is not unimodal.

of Figure 7, the $\chi_1$ values corresponding to the local minima of eq 5 are plotted against the time-average value of $\chi_1$ in the simulation. Small circles indicate residues for which no ambiguity arises; larger circles and squares are used to indicate the global and local minima, respectively, in cases where an ambiguity exists. Symbols with an inscribed + sign indicate that the $\chi_1$ distribution in the simulation is not clearly unimodal. The left panel of Figure 7 demonstrates that the agreement between $\chi_1^{fit}$ corresponding to the local minima of eq 5 and $\chi_1$ is either very good, which is predominantly the case, or very poor, which occurs much less often. In all but 3 of the 13 cases for which the agreement is poor, the $\chi_1^{fit}$ is one of the two close fits (to the coupling constant), the other of which is in good agreement with $\langle\chi_1\rangle$. The $\chi_1$ distributions of the three residues (Arg-1, Leu-29, and Arg-42) for which there is no ambiguity (and yet poor agreement between $\chi_1^{fit}$ and $\langle\chi_1\rangle$ are not unimodal and exhibit the (three) largest rms $\chi_1$ values (see below).

A similar analysis of the time-average coupling constants can be carried out by using a Gaussian model for the torsion angle distribution. A Gaussian distribution corresponds to a harmonic torsional potential and so is a reasonable first approximation. Coupling constants computed by using this model distribution depend on $m$, the mean of the Gaussian dihedral angle distribution (denoted $m$ in order to distinguish it from the time-average value of $\chi_1$ in the simulation), and $\sigma$, rms value of the distribution:

$$J(\chi_1, \sigma) = \frac{1}{\sigma\sqrt{2\pi}} \int e^{-(\theta-\chi_1)^2/2\sigma^2} J(\theta)\, d\theta \quad (6)$$

The goodness of fit is now represented by a surface:

$$F(\chi_1, \sigma) = [J(\chi_1 - 120°, \sigma) - J_{\alpha\beta_1}]^2 + [J(\chi_1, \sigma) - J_{\alpha\beta_2}]^2 \quad (7)$$

Regions of $\chi_1$, $\sigma$ space which correspond to good fit between the model distribution and time-average coupling constants from the simulation can be identified by contour plots, some examples of which are shown in Figure 8. Since a fixed-angle model can be treated as an infinitely narrow Gaussian distribution, the intersection of the contours with the $\sigma = 0$ axis corresponds to the values of $\chi_1$ which lead to good fits of a single site model to the time-average coupling constants; these results correspond to columns 6 and 7 of Table III. The local minima on the $\chi_1$, $\sigma$ surfaces computed from the time-average $\alpha\beta$ coupling constant pairs are summarized in Table III

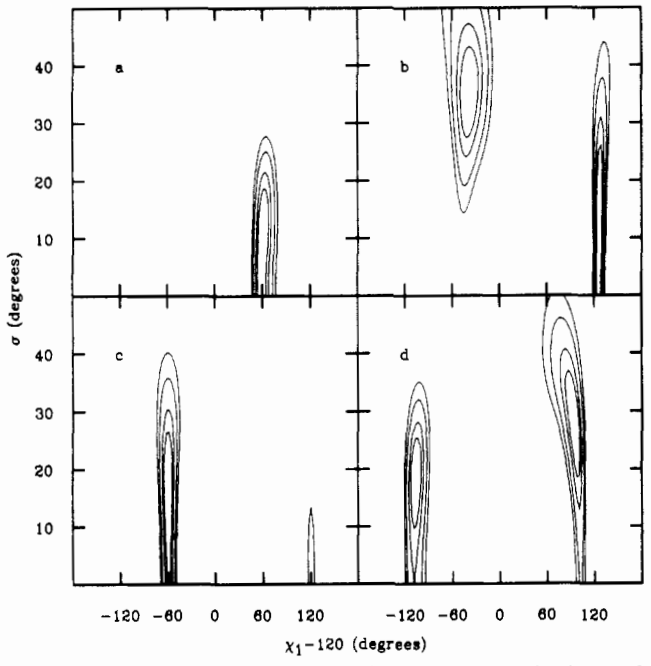


FIGURE 8: Trial function contours (eq 7) showing the level of agreement between $\alpha\beta_1$ and $\alpha\beta_2$ coupling constants computed by using a Gaussian $\chi_1$ distribution and the time-average values of the coupling constants computed from the simulation. Contours drawn at 0.5, 1.0, 2.0, and 3.0 $Hz^2$. (a) Tyr-23; (b) Leu-29; (c) Cys-38; (d) Met-52.

(columns 8 and 9) and the right panel of Figure 7. As expected, the number of residues for which an ambiguity arises due to local minima with similar values of the goodness of fit is larger than for the analysis based on a fixed-angle model. In all but two of these cases, one of the good fits to the coupling constants agrees well with $\langle\chi_1\rangle$. The exceptions are Arg-1 and Leu-29, which in the case of the fixed-angle model resulted in unambiguous fits that were very different from $\langle\chi_1\rangle$ (see above). The third residue for which the fixed-angle model yields an unambiguous, but poor, fit to $\langle\chi_1\rangle$, Arg-42, yields two close fits when the Gaussian model is applied, one of which is in good agreement with $\langle\chi_1\rangle$. There are no instances of unambiguous fits of the Gaussian model to the time-average coupling constants in poor agreement with the $\langle\chi_1\rangle$ values, in contrast to the fixed-angle model. In most instances, however, the $\chi_1^{fit}$ values obtained by using the fixed-angle or Gaussian models are similar.

It is of interest to compare the $\sigma$ values obtained by fitting the Gaussian model (eq 6 and 7) to the coupling constants with the actual rms value of $\chi_1$ from the simulation. When the $\chi_1$ distribution is unimodal, the two results are in excellent agreement (see Table III and Figure 9). This suggests that coupling constant values can be used to obtain information about dihedral angle fluctuations under ideal conditions. For nonunimodal distribution, the situation is more complicated. Figure 9 shows that in these cases, there is no simple relationship.

The fixed-angle and Gaussian models show similar trends in their ability to characterize the actual $\chi_1$ distribution. For both models, the large discrepancies correspond either to residues with nonunimodal $\chi_1$ distributions or to cases for which good fits are obtained for two different values of $\chi_1$. Goodness of fit does not distinguish nonunimodal $\chi_1$ distributions using either model. The presence of an ambiguity in the analysis is suggestive of nonunimodal $\chi_1$ distributions, however, since each of the residues with nonunimodal $\chi_1$ distributions exhibits an ambiguity in the analysis of the time-average coupling constants with one or both models. A

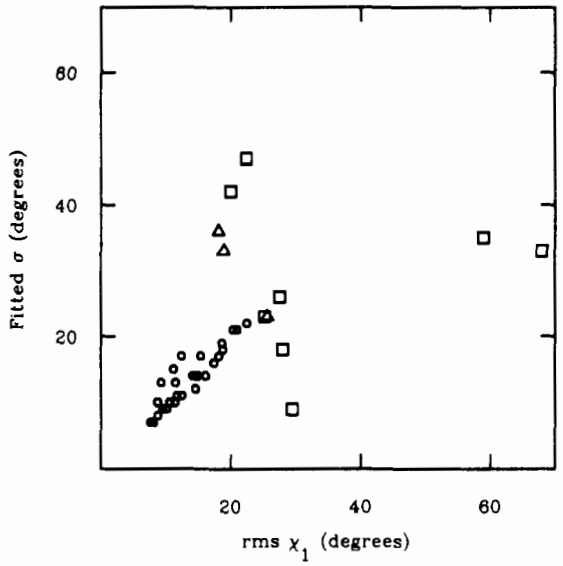


FIGURE 9: Angular distribution of $\chi_1$, obtained from coupling constants (fitted $\sigma$) and computed directly from the simulation $\langle\Delta\chi_1^2\rangle^{1/2}$. The small filled circles correspond to residues with unimodal $\chi_1$ distributions. Triangles indicate a second close fit. Squares indicate residues with multimodal $\chi_1$ distributions.

characteristic of all the cases with more than one close fit to the coupling constants is that the corresponding $\chi_1$ values are widely different.

Alternatives to fixed-angle or Gaussian model distributions in the analysis of coupling constants are limited since the number of free parameters must be limited to two (and even then ambiguities can arise). One model which has been applied extensively to the analysis of coupling constants for peptides and small organic molecules is a three-site model in which the three sites are fixed at dihedral angle values at ±60° and 180° (the staggered configurations) and the relative populations of the three sites are determined from two coupling constants and the normalization constraint on the populations (Feeney, 1975; Bystrov, 1976). It is clear from the simulations and from X-ray evidence that although protein side chains can have a number of discrete minima in their torsional potentials, these are not constrained to the classical staggered configurations. This reflects the influence of nonbonded interactions in the interior of the protein (Gelin & Karplus, 1979). The three-site model is thus inappropriate for the general analysis of vicinal coupling constants in proteins.

(*b*) *Temperature Dependence of Coupling Constants.* Each type of model torsion angle distribution carries with it implications for the temperature dependence of vicinal coupling constants. For the three-site model, changes in the relative populations of gauche and anti configurations with temperature are possible. For a Gaussian single-site model, changes in either $\chi_1$ or $\sigma$ with temperature can occur.

The observation of temperature-dependent vicinal coupling constants has been suggested as an indication of significant populations for more than one rotamer (Feeney, 1975). Although standard three-site models are not appropriate for proteins, it is clear from the dynamics that nonunimodal distributions do occur. Assuming a two-site model with known values of the coupling constant for the two sites, the average coupling constant depends on the temperature and the relative potential energies of the two configurations through the Boltzmann relation:

$$J = J_1 e^{-\Delta E/kT}/(1 + e^{-\Delta E/kT}) + J_2/(1 + e^{-\Delta E/kT}) \quad (8)$$

where $J_1$ and $J_2$ are the coupling constants for the two con-

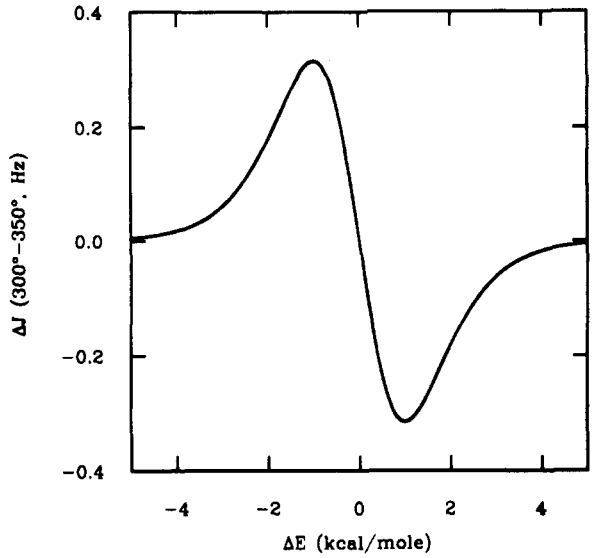


FIGURE 10: Temperature dependence of the coupling constant for two-site exchange. The difference between the coupling constants at 300 and 350 K is plotted as a function of the potential energy difference between the two sites. The two sites correspond to $\theta_1$ = 180° ($J_1$ = 12.4 Hz) and $\theta_2$ = 60° ($J_2$ = 3.25 Hz).

figurations, the exponential terms are the fractional populations, and $\Delta E$ is the potential energy difference between the two configurations. The range of temperatures for which vicinal coupling constants in proteins can be measured is relatively narrow, since they denature at high temperatures, and their proton resonances become too broad at low temperatures. The differences between coupling constants at 300 and 350 K are plotted in Figure 10 as a function of $\Delta E$ between the two configurations, assuming values of 12.4 and 3.25 Hz for $J_1$ and $J_2$, respectively, values which give the largest difference between $J_1$ and $J_2$ for the parameters ($A$, $B$, and $C$) used. If the detection limit for changes in the coupling constant with temperature is assumed to be 0.1 Hz, the range of $\Delta E$ values which will give rise to a detectable temperature dependence over the range 300–350 K is limited to $0.2 < |\Delta E| < 2.5$ (Figure 10). For $|\Delta E| < 0.2$ kcal/mol, the populations are nearly equivalent, and for $|\Delta E| > 2.5$ kcal/mol, only one rotamer is significantly populated.

A single Gaussian model torsion angle distribution can give rise to temperature-dependent vicinal coupling constants through changes in the width ($\sigma$) or the center ($m$) of the distribution. A Gaussian distribution corresponds to a harmonic potential of mean force, $E(\theta) = (k_\theta/2)(\theta - m)^2$, where $k_\theta$ is the torsional force constant and $m$ is the average value of the torsion angle. The width of the distribution depends on the temperature, $\sigma^2 = k_B T/k_\theta$, where $k_B$ is the Boltzmann constant and $T$ is the temperature. If it is assumed that the potential of mean force, and hence $k_\theta$, is independent of temperature, a torsion angle distribution which has a $\sigma$ value of 15° at 300 K will have a $\sigma$ value of 16.2° at 350 K. By use of the values of $A$, $B$, and $C$ in eq 1 which give $J(180°)$ = 12.4 and $J(60°)$ = 3.24, the 300 and 350 K values of the coupling constant with $m$ = 180° are 11.75 and 11.65 Hz, respectively. For $m = \pm 60°$, the values are 3.57 and 3.62 Hz, respectively. The temperature dependence, although small, is of the same order as the temperature dependence calculated above for the two-site model. Either of these mechanisms is sufficient to explain the magnitude of the experimental temperature dependence reported by Nagayama for BPTI (Nagayama, 1981); the reported variation of one coupling constant by 4 Hz between 30 and 85 °C is far outside the range expected from dynamics and suggests a structural change (see below).

Another possible mechanism for the temperature dependence of vicinal coupling constants is a change in the average structure with temperature. Without knowledge of the details of the structural changes with temperature, it is impossible to assess this mechanism as a source of temperature-dependent coupling constants. Specific structural changes (e.g., major population of a different dihedral angle minimum) could result in large coupling constant differences. However, there is no a priori reason to suppose that changes in the average structure with increasing temperature will result in small coupling constants becoming larger and large coupling constants becoming smaller. By contrast, this is the behavior expected from a two-site model or when changes in the width of the torsion angle distribution are responsible for the temperature dependence, as was shown above. Qualitative distinction between the different processes can perhaps be made if systematic behavior of this type is observed.

The accuracy of structural interpretations of vicinal coupling constants depends on the accuracy of the parameters $A$, $B$, and $C$ in eq 1, as well as on the model used for the torsion angle distribution. The parameters are often obtained from studies of cyclic systems (DeMarco et al., 1978) or other molecules in which some of the torsion angles are constrained to fixed values by molecular topology. Some motional averaging occurs even in these systems, and the values of $A$, $B$, and $C$ are correspondingly averaged. As an example of the magnitude of this effect, the values of $A$, $B$, and $C$ which are obtained from a least-squares fit of eq 1 to a curve obtained by weighting eq 1 by a Gaussian dihedral angle distribution with $\sigma$ = 5° and $A$, $B$, and $C$ equal to 9.4, −1.4, and 1.6 Hz, respectively, are 9.26, −1.39, and 1.67 Hz. For $\sigma$ = 10°, the values obtained are 8.84, −1.38, and 1.88 Hz.

## Discussion

Comparison of experimental coupling constants for proteins with values computed from an X-ray crystal structure corresponds to a comparison of time-average coupling constants (experimental values) with average structure results (crystal structure values). Although the data available for proteins are limited, there is evidence that the relationship between time-average and average structure coupling constants predicted from the simulations is manifested in the experimental coupling constants. Some results for BPTI and lysozyme ($J_{N\alpha}$ and $J_{\alpha,\beta}$) are given in Figure 11 (Nagayama, 1981; Delepierre et al., 1982). It is clear that there is a correlation between the experimental coupling constants and those calculated from the X-ray structure, reflecting the similarity of the average structure in solution and in the crystal. Considering first the results for $J_{N\alpha}$ (Figure 11a,c), involving $\phi$ (the main-chain angle), comparison with Figure 5a shows a much better correlation in the simulation than in the experiments. This could be due to significant differences between the solution and X-ray structures, more motion in the actual molecule than in the simulation, or errors in the measured coupling constants. It seems to us that the third alternative is most likely for $J_{N\alpha}$.

For coupling constants involving the side-chain angle $\chi_1$ ($J_{\alpha\beta}$), the experimental data (Figure 11b,d) show the general trend expected from a correspondence between the X-ray and solution structures. However, there are significant deviations, with the small coupling constants tending to have experimental values larger than predicted from the X-ray structure and the large coupling constants tending to have smaller values than predicted. In the simulation results, such deviations arise from the existence of more than one rotameric state. This suggests that multiple rotameric states for side chains are more common

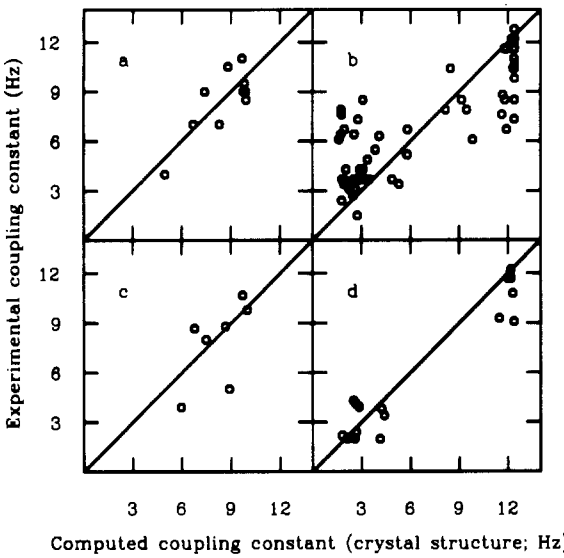


FIGURE 11: Comparison of experimental coupling constants with values computed from the X-ray crystal structure: (a) BPTI, $J_{N\alpha}$; (b) BPTI, $J_{\alpha\beta}$; (c) HEWL, $J_{N\alpha}$; (d) HEWL, $J_{\alpha\beta}$. The BPTI results are from Nagayama (1981), and the HEWL results are from Delepierre et al. (1982).

in proteins than is indicated by the published X-ray results. Only very few side chains with more than one position have been reported [e.g., see Frauenfelder et al. (1979)], but this may be a consequence of inadequacies of the available X-ray data and the difficulty in ascertaining that multiple occupancy is present; e.g., surface side chains such as lysines often are not visible in the density maps. In fact, comparison of the simulation and experimental results (Figure 5b vs. Figure 11b) leads to the conclusion that multiple rotamers are *more* common in reality than found in the calculation. This may, in part, be a consequence of the finite simulation times, since as already mentioned rotameric transitions are rare events on the dynamics time scale.

Nagayama & Wüthrich (1981) compared pairs of $\beta$-methylene coupling constants ($J_{\alpha\beta_1}$ and $J_{\alpha\beta_2}$) measured for BPTI with the correlations expected for two limiting cases: (1) fixed torsion angles (Figure 12, solid line), and (2) torsion angles distributed uniformly over ±30° about a mean value (Figure 12, dashed line). Experimental points which fall on the solid curve or in the narrow region between the solid curve and the dashed curve were described as consistent with a torsion angle distribution characterized by small fluctuations about a single value (unimodal). Points located in the region bounded by the peripheral branches of the dashed curve and the inner portion of the solid curve were described as characteristic of averaging between two or more distinct values of $\chi_1$. Points falling within the band formed by the inner portions of the solid and dashed curves were described as ambiguous. The time-average values of the $J_{\alpha\beta_1}$ and $J_{\alpha\beta_2}$ methylene coupling constants computed for the SOLV trajectory are plotted in Figure 12: the squares correspond to residues which exhibit significant populations of more than one $\chi_1$ value, and the circles correspond to residues with $\chi_1$ values distributed about a single value (unimodal). The average coupling constants computed from the simulation are seen to be generally consistent with the analysis of Nagayama and Wüthrich, although the segregation into different classes is not as simple as in their model. It is also worth noting that more realistic distributions exhibit more extensive ambiguous regions in the correlation diagram than the uniform (±30°) case considered by Nagayama and Wüthrich; e.g., the dash–dot line in Figure 12 corresponds to a Gaussian distribution with $\sigma = 25°$.

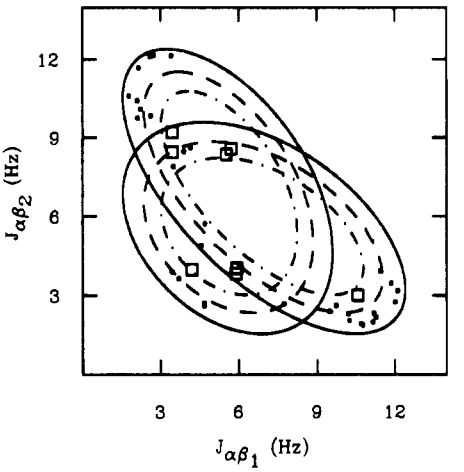


FIGURE 12: Correlation diagram for $\alpha\beta_1$ and $\alpha\beta_2$ coupling constants. Curves correspond to coupling constants computed by using eq 1 and assuming a difference of 120° between the $\alpha\beta_1$ and $\alpha\beta_2$ dihedral angles, with one of the following $\chi_1$ model distributions: (solid line) fixed; (dashed line) uniform distribution ±30° about the central value; (dot–dash line) Gaussian distribution with $\sigma = 25°$. Time-average coupling constants from the simulation are plotted as squares if more than one rotamer of $\chi_1$ is significantly populated and as filled circles if a single rotamer is populated.

In the discussion so far, it has been established that motional averaging of the type observed in the dynamics simulations is compatible with available experimental results and provides explanations for a number of features of the data. Further, it has been demonstrated that analysis of coupling constants is an important means of comparing dynamics simulations with the behavior of a protein in solution. The calculated results also enable conclusions to be drawn regarding the value of coupling constants for the experimental determination of the structure and dynamics of proteins.

In a situation where the structure of a protein is unknown, the present results show that motional averaging of the type seen in the simulations will not prevent use of $J_{N\alpha}$ values for determining possible values of the $\phi$ torsion angles when a single-site or Gaussian model is appropriate. In the dynamics simulation, the distributions of $\phi$ are all approximately Gaussian about a single potential minimum. Although there will not, in general, be a unique value of $\phi$ defined by $J_{N\alpha}$, one of the allowed values will correspond closely to the average value of $\phi$ in the protein. From the simulation, the same conclusions are generally valid for $\chi_1$; in nearly every case (see Table III), the value of $J_{\alpha\beta}$ corresponded to a torsion angle close to the average value of $\chi_1$, although ambiguities exist, as for $J_{N\alpha}$, unless stereochemical assignments for both $J_{\alpha\beta_1}$ and $J_{\alpha\beta_2}$ are available. As the fluctuations become larger and particularly when more than one rotameric state becomes significantly populated, the approach becomes less reliable. Some of these cases were found for $J_{\alpha\beta}$. Further, as one moves out along the side chain of a residue, the torsion angle fluctuations tend to increase, and the coupling constant analysis, if used by itself, becomes less effective. In any case, the description of the structure of a protein in solution must be consistent with the coupling constant data. However, coupling constants are used to maximum advantage as a structural technique when analyzed in conjunction with other data, such as those provided by nuclear Overhauser effect measurements or conformational energy calculations and dynamic simulations.

In certain situations, experimental coupling constant data alone may be sufficient to directly indicate molecular fluctuations. This is the case, for example, when both $J_{\alpha\beta_1}$ and $J_{\alpha\beta_2}$

have values near 6.5 Hz; no single torsion angle is consistent with these values. In most situations, this will not be the case, and other approaches are needed to extract dynamical information. One approach is to combine the coupling constant analysis with other data, such as cross-relaxation rates from nuclear Overhauser effects. Another approach of particular interest is possible where the average protein structure in solution is known. For small, stable proteins such as BPTI and lysozyme, considerable evidence supports the close similarity of the average structures in solution and in crystals. If this similarity can be assumed, the analysis in this paper indicates that when agreement between experimental coupling constants and those calculated from the crystal structure is poor, the torsion angle distribution is not about a single potential minimum and that jumps between different conformers occur. For the cases where agreement is good, fluctuations that do occur are about a single potential well. A fit of the measured coupling constants to the average torsion angle and a Gaussian distribution about that average then provides an excellent description of the magnitude of the torsion angle fluctuations.

In conclusion, it is hoped that the analysis of coupling constant fluctuations provided by molecular dynamics simulations will sere as a useful guide to future experimental studies in this area.

## ACKNOWLEDGMENTS

We are indebted to Muriel Delepierre, Toshiko Ichiye, Edward Olejniczak, Flemming Poulsen, and Christina Redfield for numerous illuminating discussions and to S. Cutler for assistance in preparing the manuscript.

**Registry No.** BPTI, 12407-79-3; HEWL, 9001-63-2.

## REFERENCES

Artymiuk, P. D., Blake, C. C. F., Grace, D. E. P., Oatley, S. J., Phillips, D. C., & Sternberg, M. J. E. (1979) *Nature (London) 280*, 563.

Barfield, M., & Karplus, M. (1969) *J. Am. Chem. Soc. 91*, 1.

Brooks, B., Bruccoleri, R., Olafson, B., States, D., Swaminathan, S., & Karplus, M. (1983) *J. Comput. Chem. 4*, 187.

Bystrov, V. F. (1976) *Prog. Nucl. Magn. Reson. Spectrosc. 10*, 41.

Bystrov, V. F., Ivanov, V. T., Portnova, S. L., Balashova, T. A., & Ouchinnikov, Y. A. (1973) *Tetrahedron 29*, 873.

Campbell, I. D., Dobson, C. M., Moore, G. R., Perkins, S. J., & Williams, R. J. P. (1976) *FEBS Lett. 70*, 96.

Cung, M. T., & Marraud, M. (1982) *Biopolymers 21*, 953.

Delepierre, M., Dobson, C. M., & Poulsen, F. M. (1982) *Biochemistry 21*, 4756.

DeMarco, A., Llinâs, M., & Wüthrich, K. (1978) *Biopolymers 17*, 617.

Dobson, C. M. (1977) in *NMR in Biology* (Dwek, R. A., Campbell, J. D., Richards, R. E., & Williams, R. J. P., Eds.) p 63, Academic Press, London.

Dubs, A., Wagner, G., & Wüthrich, K. (1979) *Biochim. Biophys. Acta 577*, 177.

Feeney, J. (1975) *Proc. R. Soc. London, A 345*, 61.

Frauenfelder, H., Petsko, G. A., & Tsernoglou, D. (1979) *Nature (London) 280*, 558.

Gelin, B. R., & Karplus, M. (1979) *Biochemistry 18*, 1256.

Gibbons, W. A., Nêmethy, G., Stern, A., & Craig, L. C. (1970) *Proc. Natl. Acad. Sci. U.S.A. 67*, 239.

Hoch, J. C. (1983) Ph.D. Thesis, Harvard University.

Hoch, J. C., Dobson, C. M., & Karplus, M. (1982) *Biochemistry 21*, 1118.

IUPAC–IUB Commission on Biochemical Nomenclature (1970) *J. Mol. Biol. 52*, 1.

Karplus, M. (1959) *J. Chem. Phys. 30*, 11.

Karplus, M. (1963) *J. Am. Chem. Soc. 85*, 2870.

Karplus, M., & McCammon, A. (1981) *CRC Crit. Rev. Biochem. 9*, 293.

Karplus, M., & McCammon, A. (1983) *Annu. Rev. Biochem. 53*, 263.

Kopple, K. D., Wiley, G. R., & Tauke, R. (1973) *Biopolymers 12*, 627.

McQuarry, D. A. (1976) *Statistical Mechanics*, Harper and Row, New York.

Nagayama K. (1981) *Adv. Biophys. 14*, 139.

Nagayama, K., & Wüthrich, K. (1981) *Eur. J. Biochem. 115*, 653.

Northrup, S. H., Pear, M. R., McCammon, J. A., & Karplus, M. (1980) *Nature (London) 286*, 304.

Poulsen, F. M., Hoch, J. C., & Dobson, C. M. (1980) *Biochemistry 19*, 2597.

Tonelli, A. E., Brewster, A. I., & Bovey, F. A. (1970) *Macromolecules 3*, 412.

van Gunsteren, W. F., & Karplus, M. (1982) *Biochemistry 21*, 2259.

Wagner, G., & Wüthrich, K. (1982) *J. Mol. Biol. 155*, 347.